Materials Research. 2014; 17(6): 1466-1473
DOI: http://dx.doi.org/10.1590/1516-1439.289214

Thermal Inkjet Printing of Copper Tetrasulfonated Phthalocyanine (CuTsPc) as a Semiconducting Layer on Flexible MIS Capacitors

Tiago Carneiro Gomes[a]*, Rafael Furlan de Oliveira[a], Carlos José Leopoldo Constantino[a], Marcelo Marques da Silva[a], Élder Mantovani Lopes[b], Neri Alves[a]

[a]Department of Physics, Chemistry and Biology, Faculty of Sciences and Technology – FCT, São Paulo State University – UNESP, Presidente Prudente, SP, Brazil
[b]Federal Institute of Education, Science and Technology of Santa Catarina – IFC, Araquari, SC, Brazil

Received: April 9, 2014; Revised: November 21, 2014

Thermal inkjet-printing of copper tetrasulfonated phthalocyanine (CuTsPc) films containing polyvinyl alcohol (PVA) plasticizer were used to fabricate flexible metal-insulator-semiconductor (MIS) capacitors using anodic aluminum oxide (Al_2O_3) as the insulating layer. The Al_2O_3 layer and printed CuTsPc+PVA films were characterized individually and in a MIS structure by electrical impedance spectroscopy. Capacitance-frequency and capacitance-voltage measurements revealed distinct contributions from CuTsPc and PVA on the device electrical response. From these measurements the semiconductor charge carrier mobility, μ, of 1.22×10^{-4} cm^2 V^{-1} s^{-1} and the doping density, N_A, of 3.1×10^{16} cm^{-3} were calculated. It was observed a low-frequency electrical response, which was attributed to diffusional processes within the printed film arising from Na^+ ions dissociated from the CuTsPc molecule. A simple equivalent circuit model was proposed to take this effect into account. Finally, the results shown here demonstrate the possibility to produce flexible organic electronic devices exploiting the semiconducting properties of water-soluble CuTsPc molecules using low-cost commercial printers.

Keywords: *thermal inkjet printing, copper tetrasulfonated phthalocyanine, anodic aluminum oxide, MIS capacitors, organic electronics*

1. Introduction

Organic materials have been studied for years as active compounds for many electronic purposes as the fabrication of field-effect transistors (OFETs)[1-3], photovoltaics (OPVs)[4-6], sensors[7-10], memories[11-13], radio-frequency identification tags (RFIDs)[14,15] and light-emitting diodes (OLEDs)[16-18]. Such applications become even more interesting when solution-processed organic materials are used to produce low-cost and flexible devices, which can be achieved by printing techniques, for instance[19-21]. However, to succeed in the printing of organic devices with suitable electrical characteristics, the development of strategies to improve material properties is extremely important[20,22]. Previously, we demonstrated an ink formulation to print aqueous-insoluble polyaniline (PANI) using a commercial thermal desktop printer[22]. In that approach the use of organic solvents (viz. N-methyl-2-pyrrolidone, ethylene glycol and isopropanol) with ultrapure water allowed the formulation and printing of PANI solution similarly to the preparation and printing of standard inks for commercial printers. In the literature other strategies reporting ink formulation of different materials for thermal inkjet (TIJ) printing can also be found[23-26].

TIJ printing is an attractive method that exhibits advantages such as accurate droplet positioning, minimal waste production, reasonable printing speeds and compatibility with different flexible substrates and materials[21,22]. Additionally, the use of commercial desktop printers is very versatile for rapid device prototyping and patterning at real low-cost production[20-22]. The TIJ technique, however, requires the use of water-based materials (inks) with very specific properties such as appropriate viscosity (ca. 2.5 mPas), surface tension (ca. 33 mN m^{-1}) and boiling point (ca. 90–95 °C)[21,22]. Thus, the fine tuning of material properties is mandatory to fulfill these particular characteristics, which can be achieved through the formulation and modification of standard materials. In this context, water-soluble organic semiconductors (OSC), especially phthalocyanine molecules containing sulfonate groups, can be a very attractive candidate for organic electronic devices produced by TIJ printing.

Sulfonated-substituted phthalocyanines have been exploited mainly in OFETs[27-29] and OPVs[4-6,30]. Regarding OFETs, Locklin et al.[27] have produced devices with ambipolar-like behavior using the layer-by-layer (LbL) technique to assemble thin films of cationic and anionic copper phthalocyanine derivatives. They have shown charge carrier mobilities in the range of 10^{-4} to 10^{-6} cm^2 V^{-1} s^{-1} for both p- and n-type channels depending the fabrication conditions[27]. Chaidogiannos et al.[28] have verified charge carrier mobilities of approximately 0.2 cm^2 V^{-1} s^{-1} for cobalt tetrasulfonated phthalocyanine (CoTsPc)-based spincoated devices whereas non-substituted counterparts have shown

*e-mail: tiagocunesp@gmail.com.br

mobilities of 10^{-4} cm^2 V^{-1} s^{-1}. According to the authors, the device field-effect mobility is controlled by the presence of Na^+ which depends on the degree of sulfonation of the CuTsPc molecule[28]. In OPVs, sulfonated-substituted phthalocyanine has been used as an interlayer between indium-tin oxide (ITO) electrodes and photoactive polymer blends[30] as well as a donor layer in fullerene-based devices[4]. Benten et al.[6] used LbL method to exploit the characteristics of copper tetrasulfonated phthalocyanine (CuTsPc) in order to obtain power conversion efficiencies (PCE) of 0.01% and open-circuit voltages (V_{OC}) of approximately 0.4 V, whereas Schumann et al.[4] obtained PCE of 0.32% and V_{OC} of 0.6 V for spincoated CuTsPc-based devices. According to Schumann and co-workers such improved characteristics on CuTsPc OPVs arise from the presence of sulfonic acid substituents on the phthalocyanine.

All the mentioned examples about the use of water-soluble phthalocyanines on electronic devices rely on different fabrication techniques such as LbL[6,27], electrodeposition[5] and spincoating[4,28,30]. However, to the best of our knowledge, the TIJ deposition of sulfonate-substituted phthalocyanines has not been demonstrated yet for such purposes. To address information about the feasibility of TIJ printed electronic devices, flexible metal-insulator-semiconductor (MIS) capacitors based on copper tetrasulfonated phthalocyanine (CuTsPc) and anodic aluminum oxide (Al_2O_3) were fabricated. The MIS capacitor is the core of OFETs and a powerful tool for electrical characterization of OSC, dielectrics and interfaces[31-36]. Its simple structure and versatility allow the extraction of several semiconductor parameters such as conductivity, charge carrier mobility and doping density[31-35]. Here, the electrical properties of CuTsPc/Al_2O_3 MIS capacitors prepared onto flexible aluminum (Al)-coated Teflon® substrates were investigated. To provide uniformity to CuTsPc printed films, poly(vinyl alcohol) (PVA) was used as a plasticizer. Atomic force microscopy and impedance spectroscopy measurements were used to characterize the individual materials and the MIS device. Finally, the charge carrier mobility, μ, and doping density, N_A, were calculated for the CuTsPc+PVA-based device.

2. Experimental Details

2.1. Materials and instrumentation

Copper phthalocyanine-3,4',4'',4'''-tetrasulfonic acid tetrasodium salt powder, M_W 984.25 g/mol, dye content 85%, and poly(vinyl alcohol) (PVA), average Mw 130,000 g/mol, 99% hydrolyzed, were purchased from Sigma-Aldrich Ltd. All other reagents were purchased from Synth and used without further purification. Aluminum (Al)-coated Teflon® substrates (12 mm-thick) were acquired from Dilectrix (Dupont trademark).

The CuTsPc+PVA films were printed using a Hewlett-Packard (HP) thermal desktop printer (model 2460) whereas the anodization of Al-coated substrates was carried out using Keithley 2420 source-meter unit in a home-made electrochemical cell. Gold top electrodes (70 nm-thick, area of 2×10^{-6} m^2) were thermally deposited onto all samples through a shadow mask using an Edwards Auto 306 system. The samples were electrically characterized by impedance spectroscopy using a frequency response analyzer (Solartron model 1260) coupled to a dielectric interface (model 1296). Morphological investigations were carried out by atomic force microscopy (AFM) using a Nanosurf equipment (model EasyScan 2) and TAP 190 Al-G probes.

2.2. CuTsPc+PVA ink preparation and printing

To print CuTsPc+PVA films a solution containing 100 mg of CuTsPc (powder) and 2.5 mg of PVA (powder) was prepared in 5 ml ultrapure water (Millipor Milli Q system). The addition of PVA as a plasticizer is necessary to provide homogeneity to the CuTsPc film. The CuTsPc+PVA ink was sonicated for 30 min at room temperature and carefully filtered using a polytetrafluoroethylene (PTFE) syringe filter (pore size of 0.45 mm) immediately before the printing procedure. To receive the CuTsPc+PVA ink, the printer cartridge (HP number 21) was opened and cleaned with n-methyl-2-pyrrolidone (NMP), isopropyl alcohol and deionized water (1:1:1 v:v:v) and left in ultrasonic bath for 20 min to remove all residues.

The samples were designed using Microsoft Word® software. The printing parameters were set to RGB (0,0,0) at the lowest speed and maximum printing quality, which means the largest number of pixels per inch that can be achieved by the printer. The CuTsPc+PVA films were printed onto bare and Al_2O_3-coated aluminized Teflon® substrates for the CuTsPc+PVA electrical characterization and MIS capacitor fabrication, respectively.

2.3. Anodization of aluminized Teflon® substrates

Anodic Al_2O_3 was used as the dielectric layer on MIS capacitors containing CuTsPc+PVA as the semiconducting material. The Al_2O_3 dielectric layer was produced by the anodization of the thin Al coverage of Teflon® using constant electrical currents. This method allows the obtainment of barrier-type Al_2O_3 films with nanometric thicknesses and excellent insulating properties for organic electronic devices[37]. The electric field between two electrodes (viz. Al and Au) immersed in a proper solution allows O^{2-} ions from the electrolyte to reach the Al electrode surface and react with Al^{3+} ions to form Al_2O_3 according to the Equation 1[38]:

$$2Al^{3+} + 3O^{2-} \rightarrow Al_2O_3 \quad (1)$$

During the oxide growth, the system electrical resistance increases due to the Al_2O_3 insulating properties. To keep constant the electrical current flowing between the electrodes, a corresponding increase of voltage is required. This results in a compromise between the oxide layer thickness, d_{OX}, and the applied potential, V, described by the Equation 2[37]:

$$f = \frac{d_{ox}}{V} \quad (2)$$

whereas f is called anodization factor and can vary depending the experimental conditions for the oxide growth[37]. Here, 20 nm-thick Al_2O_3 films were produced in a home-made electrochemical cell containing 30 mmol L^{-1} electrolytic solution of tartaric acid, ethylene glycol and water. The

electrolyte pH was adjusted to 6.0 using low-concentrated ammonium hydroxide solution. The use of tartaric acid at pH values 6.0 - 7.0 is known to allow the formation of barrier-type Al_2O_3 films with good dielectric properties[37]. The following protocol was used for the oxide fabrication: i) a constant current of 250 μA cm^{-2} was applied between the Al-coated Teflon® and the Au electrode and ii) the electrical potential was held at the final voltage for 2 min to improve the oxide uniformity.

2.4. Sample morphological and electrical characterization

Three different samples were produced to investigate the electrical and morphological properties of involved materials. These include sandwich-like structures of i) thermally deposited Au electrodes onto anodized Al-coated Teflon® substrates (Au/Al_2O_3/Al-Teflon®); ii) thermally deposited Au electrodes onto CuTsPc+PVA films printed on Al-coated Teflon® (Au/CuTsPc+PVA/Al-Teflon®) and iii) MIS capacitor (Au/CuTsPc+PVA/Al_2O_3/Al-Teflon®), as depicted in Figure 1.

After fabrication the samples were annealed at 100 °C for 1h in vacuum to remove oxygen and water traces. AFM images were acquired in tapping mode, scanned area of 10×10 mm and analyzed using Gwyddion 2.31 software. The roughness of each sample was calculated averaging the root-mean-squared roughness of 8 regions (2x2 μm) within every image. For the electrical characterization, impedance spectroscopy measurements were carried out in moderate vacuum (approximately 10^{-1} Torr) and at room temperature. Capacitance and dielectric loss curves were obtained as a function of frequency and DC bias considering AC amplitude of 100 mV.

3. Results and Discussion

3.1. Morphological characterization

Morphological characteristics of bare Al-coated Teflon® substrates, anodic Al_2O_3 layer and printed CuTsPC+PVA film were investigated by AFM and are shown in Figures 2a, 2b and 2c, respectively.

The Figure 2a revealed an entangled fiber-like morphology of the bare Al-coated Teflon® substrate with an average roughness of (15 ± 2) nm, whereas the anodized Al_2O_3 film exhibited some corrugation coupled with smaller globular features on its surface (Figure 2b). These morphological characteristics resulted in roughness values as high as (29 ± 5) nm which can be the cause of charge traps suggested from the capacitance-frequency curve for the Al/Al_2O_3/Al-Teflon® structure (Figure 3). Printed CuTsPc+PVA films showed some agglomeration, as depicted in Figure 2c, with roughness values of approximately (17 ± 4) nm.

3.2. AC electrical characterization of flexible Al2O3 thin films

Figure 3 shows capacitance and *tanδ* curves (the latter corresponds to the dielectric loss/capacitance ratio) as a function of frequency for the 20 nm-thick Al_2O_3 film anodized onto Al-Teflon® substrates. As frequency increases, the capacitance (black line) smoothly decreases reaching constant values in the range between 10^4 – 10^5 Hz. This behavior suggests the presence of charge traps with different time responses at the Al_2O_3/Al interface as observed by

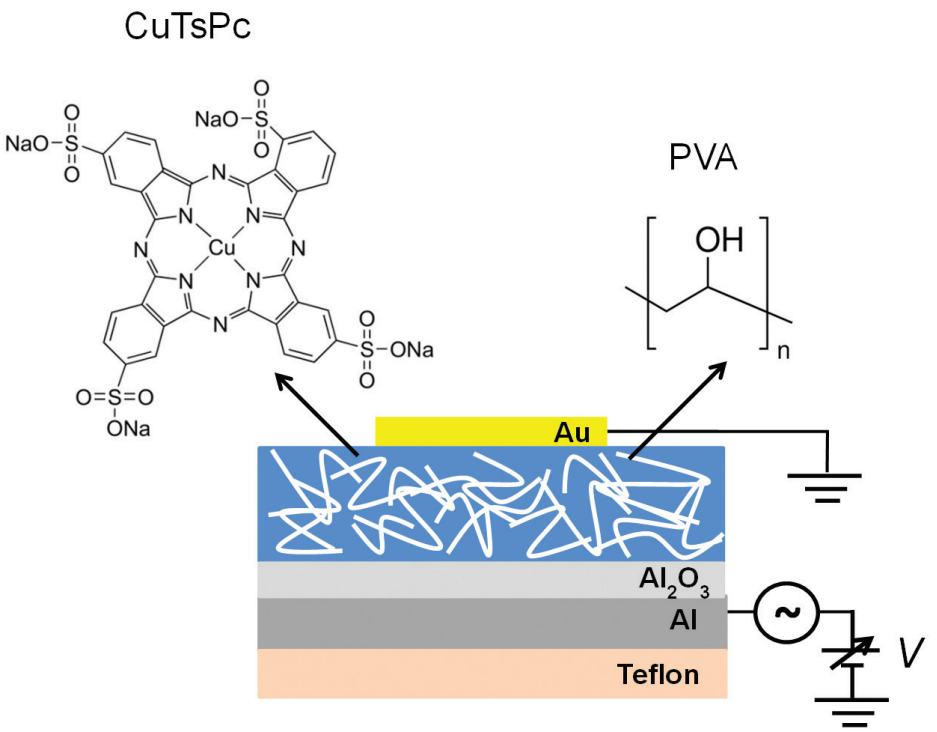

Figure 1. Schematic representation of the MIS device and the molecular structure of the respective materials.

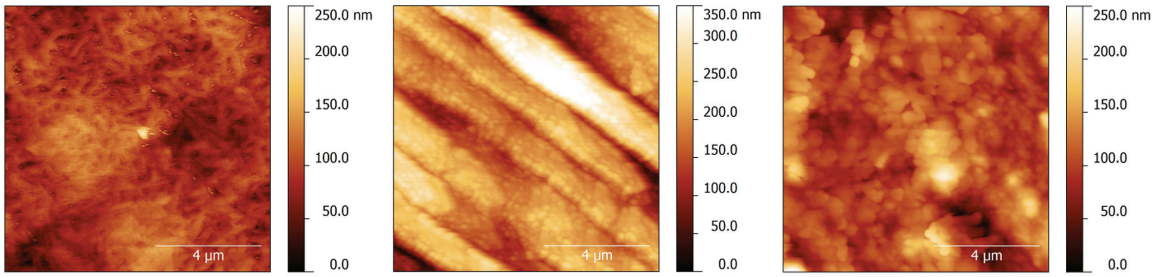

(a) (b) (c)

Figure 2. AFM images (10 × 10 mm) of a) bare Al-coated Teflon®, b) anodic Al_2O_3 layer and c) printed CuTsPc+PVA film.

Hourdakis and Nassiopoulos for capacitors containing porous alumina layer[39]. Subsidiary experiments revealed rather constant capacitance values for anodic Al_2O_3 produced onto highly pure Al films thermally evaporated (data not shown). Thus, the traps on the Al/Al_2O_3 can be related to the high roughness of the Al surface (15 ± 2 nm) and the Al_2O_3 layer (29 ± 5 nm) or even to the presence of impurities on the Al film. The dielectric constant (ε_{OX}) of the Al_2O_3 film was extract from the capacitance curve at approximately 10^4 Hz to avoid such contribution of traps obtaining $\varepsilon_{OX} = 10$, which is in agreement with previously reported values for barrier-type anodic films[39]. The *tanδ* curve (blue line) exhibited values of 10^{-2}, indicating an Al_2O_3 film with good insulating characteristics.

3.3. AC electrical characterization of printed CuTsPc+PVA films

Figure 4 depicts the capacitance and loss curves of printed CuTsPc+PVA films onto Al-coated Teflon® substrates. Here, the frequency was swept starting from very low values (10^{-2} Hz) in order to investigate the occurrence of typical low-frequency response of Na^+ ions from CuTsPc sulfonate moiety. A sharp decrease of capacitance values (black line) is observed in the range of 10^{-2} Hz to 10^2 Hz, reaching a constant behavior at higher frequencies. From these values the CuTsPc film thickness was estimated to be about 110 nm, considering 3 for the CuTsPc dielectric constant[40]. For this estimative, the contribution of PVA was not taken into account. The loss curve (blue line) revealed a relaxation peak (known as Maxwell-Wagner relaxation) at approximately 10 Hz. This is the classical electrical behavior of a capacitor with a two different dielectric layer[34,36]. Here, however, no experimental evidences that CuTsPc and PVA form discrete phases could be obtained, as shown in Figure 2c for AFM measurements, for example. From Figure 4 it is also observed that the loss values are higher at very low frequencies (ca. 10^{-2} Hz), which suggest the existence of an ionic diffusion mechanism of the Na^+ ions from CuTsPc within the printed film.

3.4. AC electrical characterization of flexible MIS capacitors

Once the electrical properties of the anodic Al_2O_3 layer and the printed CuTsPc+PVA film were evaluated, the response of CuTsPc+PVA/Al_2O_3 MIS capacitors were investigated. Figures 5a and 5b show, respectively, the device

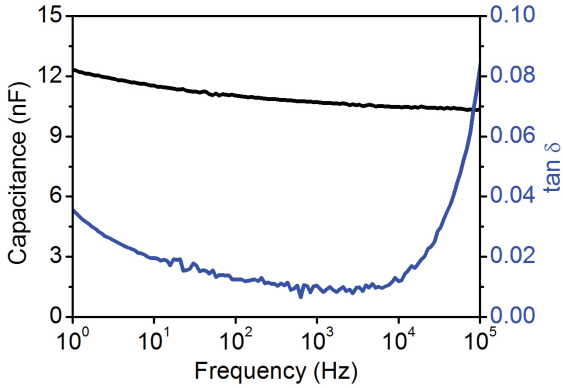

Figure 3. Capacitance-frequency and *tanδ*-frequency plots for a 20 nm-thick anodic Al_2O_3 layer measured in vacuum and at room temperature.

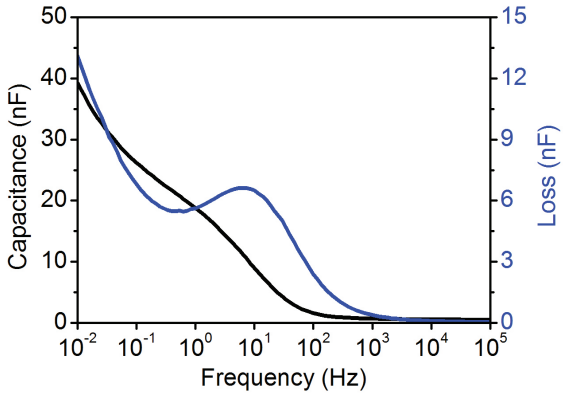

Figure 4. Capacitance-frequency and dielectric loss-frequency plots for CuTsPc+PVA film printed onto Al-coated PET substrates obtained in vacuum and at room temperature.

capacitance and loss curves as function of frequency for different DC voltages. The observed capacitance variations with frequency indicate the existence of accumulation and depletion regimes as expected for a MIS device[31-35]. On the loss plot, Maxwell-Wagner relaxation peaks are clearly present at around 1 Hz for different applied bias.

It is worth mentioning that CuTsPc+PVA printed film occupies an area close to the top Au electrode one, thus lateral currents are expected to be negligible in this device. Therefore, the capacitance increase observed at low

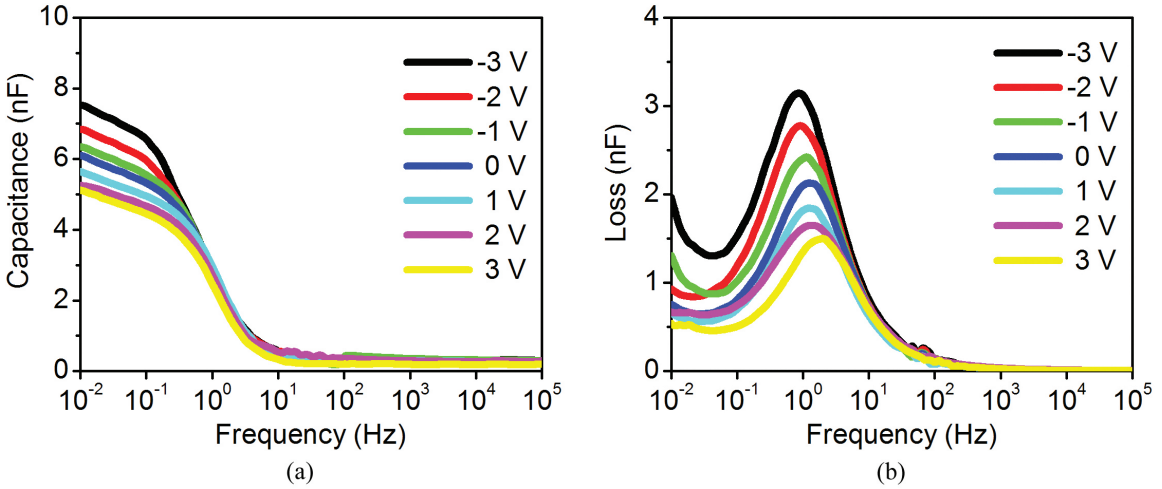

Figure 5. a) Capacitance-frequency and b) dielectric loss-frequency plots at several DC bias for CuTsPc+PVA/Al_2O_3 MIS capacitor obtained in vacuum and at room temperature.

frequencies (below 10^{-1} Hz) and its respective loss response can be attributed to the Na^+ conduction as discussed for the CuTsPc+PVA film. These capacitance and loss curves for the MIS device can be modeled using the equivalent electrical circuit shown in Figure 6.

The equivalent circuit is proposed considering: i) within the CuTsPc+PVA film there is 2.5% w/w of insulating PVA, which can cause an increase of the effective insulator thickness, therefore, the existence of a capacitance, C_P, in series to the oxide capacitance, C_O, should be taken into account; ii) there is a Maxwell-Wagner relaxation process due to the field-effect in the CuTsPc film in which the intensity varies with the DC bias and this effect is represented by C_T in parallel with R_T; iii) C_D and R_D account to the relaxation mechanism and the ionic diffusion processes in the CuTsPc+PVA films, occurring at low frequencies.

Figure 7 shows the experimental and simulated capacitance and dielectric loss curves for the MIS device. The experimental curve was obtained at accumulation regime (–3 V). The simulations were performed using Zview® software and the proposed electrical circuit.

The simulation was generated considering C_O = 8.8 nF, that corresponds to a 20 nm-thick Al_2O_3 film calculated from Figure 3. The C_P value (36 nF) was obtained considering the following approximation: as 2.5% w/w PVA within CuTsPc is present, it was considered that PVA could form a continuous insulating film as thick as 2.5% of the CuTsPc+PVA total thickness calculated from capacitance-frequency curve in Figure 5a. The R_T and C_T values were obtained from Maxwell-Wagner peak using $\omega\tau = 1$ and the Equation 3[32]:

$$f_{loss} = \frac{1}{2\pi R_T (C_T + C_O)} \quad (3)$$

The C_D e R_D values were defined taking as guideline the results shown in Figures 5a and 5b, from where the conductivity was estimated as 5.9 x10^{-9} S/m. It is important

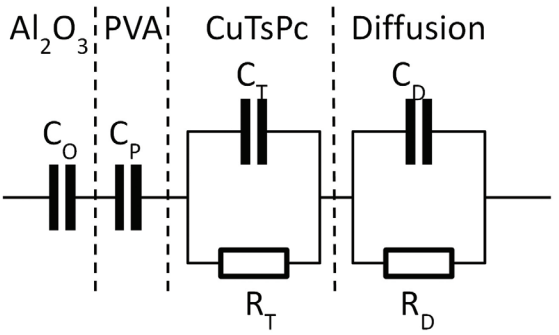

Figure 6. Equivalent circuit proposed for the MIS device. C_O, C_P, C_T stand, respectively, for the capacitances of Al_2O_3, PVA and CuTsPc layers. R_T is the electrical resistance of CuTsPc and C_M and R_M are, respectively, the capacitance and resistance terms related to ionic diffusion processes.

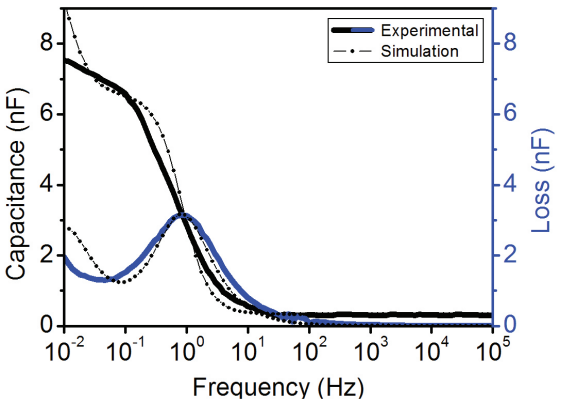

Figure 7. Experimental (solid line) and simulated (dashed line) capacitance-frequency and dielectric loss-frequency curves for the MIS device. Simulated results were obtained using the Zview® software.

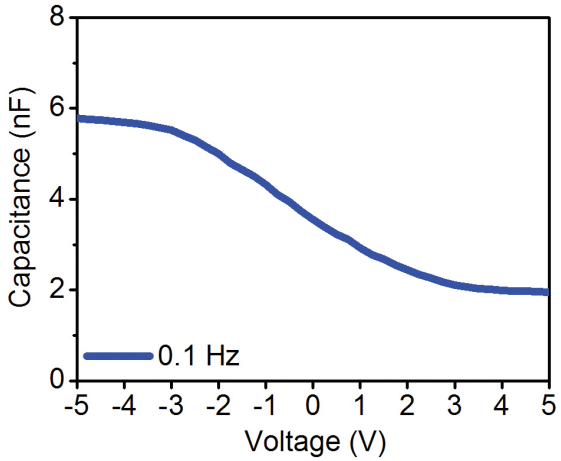

Figure 8. Capacitance-voltage plot at 0.1 Hz for the MIS device. The charge carrier density can be estimated from the region between -1 V and 1 V.

to address that the equivalent circuit analysis is not a proper fit, but a qualitative general description of the device electrical behavior in which the proposed circuit seems to be appropriated. Although such behavior agrees with the model, more conclusive studies would be necessary in order to understand the overall electrical processes, mainly those at low frequencies. Here, the most important aspect is despite the ionic diffusion process that occurs in the MIS response, as clarified by the electrical circuit representation, the typical field-effect behavior of MIS capacitors still present, as shown in Figure 8 for the device capacitance-voltage curve.

The main characteristic of MIS capacitors is that capacitance varies with DC bias[31-35]. The Figure 8 shows the capacitance-voltage curve for the CuTsPc+PVA/Al_2O_3 MIS device performed at 0.1 Hz. This frequency is intermediary to both relaxations observed in Figure 5b, where there are not inherent low frequency effects represented by the branch containing C_D and R_D in the equivalent circuit. This is an important assumption because it allows the analysis of the single contribution of CuTsPc. For negative voltages (accumulation regime) the measured capacitance of 5.8 nF corresponds approximately to the values of C_O e C_P from the insulator equivalent capacitance. For positive voltages (depletion regime), the capacitance of approximately 1.9 nF suggests that the device does not reach the complete depletion, since its capacitance in this condition should correspond to 0.5 nF (Figure 7). Therefore, despite the low frequency relaxation originated from diffusions within the CuTsPc+PVA, it is also possible to observe the field-effect and the capacitance variation with voltage at 0.1 Hz, which allows the calculation of the CuTsPc parameters.

The CuTsPc charge carrier density, N_A, was estimated to be 3.7×10^{16} cm^{-3} from the slope on the capacitance-voltage plot using the Mott-Schottky relation as shown by the Equation 4[41]:

$$N_A(w) = -2\left[q\varepsilon_s \frac{d}{dV_G}\left(\frac{1}{C_a}\right)^2\right]^{-1} \quad (4)$$

Additionally, from the Maxwell-Wagner relaxation frequency (Figure 5b) and using Equation 3, the conductivity and the mobility (μ) of the CuTsPc+PVA could be estimated as being 5.88×10^{-7} S/cm and 1.22×10^{-4} cm^2 V^{-1} s^{-1}, respectively. Here, although it was necessary to add PVA as plasticizer to provide uniformity to the CuTsPc printed film and, therefore, to guarantee a proper device operation, it is possible to obtain important parameters that characterize the semiconducting properties of CuTsPc. In this sense, new perspectives for this work include the replacement of PVA as a plasticizer matrix by conducting polymers or polyanions to promote the CuTsPc doping. This strategy might provide higher mobilities allowing the fabrication of thermally printed electronic devices with better electrical properties, as organic field-effect transistors, for instance.

4. Conclusion

The electrical characterization of printed CuTsPc films under two novel aspects, the successful thermal inkjet printing of CuTsPc onto a flexible Al_2O_3-coated substrate and the impedance spectroscopy study of the electrical properties of a CuTsPc-based MIS capacitor, is presented. Compact Al_2O_3 films with suitable electrical properties and dielectric constant (~10) were obtained by anodization process. This method can be appropriate for the fabrication of devices in which ease-processed thin dielectrics are required. To fabricate CuTsPc-based MIS capacitor, PVA was added in the CuTsPc ink to give it uniformity and homogeneity during the printing procedure. The electrical characterization of the MIS capacitor revealed the occurrence of the accumulation and depletion regimes as well a well-defined Maxwell-Wagner relaxation process. However, the absence of a constant capacitance at the accumulation regime suggests some contribution from the ionic currents in the CuTsPc+PVA response. Additionally, from the equivalent circuit analysis and the capacitance-voltage curve, it was possible to obtain the conductivity, mobility and carrier density of the device. Finally, it is shown the possibility to produce flexible MIS devices based on CuTsPc using low-cost commercial printers for applications on electronic devices. Our results contribute to the comprehension of the electrical properties of printed OSC and demonstration of the efficiency of the TIJ technique to produce low-cost prototypes.

Acknowledgements

The authors thank FAPESP and INEO (Brazil) for the financial support.

References

1. Tsumura A, Koezuka H and Ando T. Macromolecular Electronic Device: Field-effect Transistor with a Polythiophene Thin Film. *Applied Physics Letters*. 1986; 49(18):1210-1212. http://dx.doi.org/10.1063/1.97417.
2. Wang C, Dong H, Hu W, Liu Y and Zhu D. Semiconducting π-conjugated systems in field-effect transistors: a material odyssey of organic electronics. *Chemical Reviews*. 2012; 112(4):2208-2267. http://dx.doi.org/10.1021/cr100380z. PMid:22111507
3. Muccini M. A bright future for organic field-effect transistors. *Nature Materials*. 2006; 5(8):605-613. http://dx.doi.org/10.1038/nmat1699. PMid:16880804
4. Schumann S, Hatton R and Jones TS. Organic photovoltaic devices based on water-soluble copper phthalocyanine. *The Journal of Physical Chemistry C*. 2011; 115(11):4916-4921. http://dx.doi.org/10.1021/jp109544m.
5. Luo X, Xu L, Xu B and Li F. Electrodeposition of Zinc Oxide/Tetrasulfonated Copper Phthalocyanine Hybrid Thin Film for Dye-sensitized Solar Cell Application. *Applied Surface Science*. 2011; 257(15):6908-6911. http://dx.doi.org/10.1016/j.apsusc.2011.03.029.
6. Benten H, Kudo N, Ohkita H and Ito S. Layer-by-layer deposition films of copper phthalocyanine derivative: their photoelectrochemical properties and application to solution-processed thin-film organic solar cells. *Thin Solid Films*. 2009; 517(6):2016-2022. http://dx.doi.org/10.1016/j.tsf.2008.09.102.
7. Volpati D, Alessio P, Zanfolim AA, Storti FC, Job AE, Ferreira M, et al. Exploiting distinct molecular architectures of ultrathin films made with iron phthalocyanine for sensing. *The Journal of Physical Chemistry B*. 2008; 112(48):15275-15282. http://dx.doi.org/10.1021/jp804159h. PMid:18989908
8. Khodagholy D, Doublet T, Quilichini P, Gurfinkel M, Leleux P, Ghestem A, et al. In vivo recordings of brain activity using organic transistors. *Nature Communications*. 2013; 4:1575-1582. http://dx.doi.org/10.1038/ncomms2573. PMid:23481383
9. Casalini S, Leonardi F, Cramer T and Biscarini F. Organic field-effect transistor for label-free dopamine sensing. *Organic Electronics*. 2013; 14(1):156-163. http://dx.doi.org/10.1016/j.orgel.2012.10.027.
10. Torsi L, Magliulo M, Manoli K and Palazzo G. Organic field-effect transistor sensors: a tutorial review. *Chemical Society Reviews*. 2013; 42(22):8612-8628. http://dx.doi.org/10.1039/c3cs60127g. PMid:24018860
11. William S, Mabrook MF and Taylor DM. Floating-gate memory based on an organic metal-insulator-semiconductor capacitor. *Applied Physics Letters*. 2009; 95(9):093309. http://dx.doi.org/10.1063/1.3223606.
12. Lian K, Li R, Wang H, Zhang J and Gamota D. Printed flexible memory devices using copper phthalocyanine. *Materials Science and Engineering B*. 2010; 167(1):12-16. http://dx.doi.org/10.1016/j.mseb.2010.01.020.
13. Ávila-Niño JA, Machado WS, Sustaita AO, Segura-Cardenas E, Reyes-Reyes M, López-Sandoval R, et al. Organic low voltage rewritable memory device based on PEDOT:PSS/f-MWCNTs thin film. *Organic Electronics*. 2012; 13(11):2582-2588. http://dx.doi.org/10.1016/j.orgel.2012.07.034.
14. Lakafosis V, Rida A, Vyas R, Yang L, Nikolaou S and Tentzeris MM. Progress towards the first wireless sensor networks consisting of inkjet-printed, paper-based, rfid-enabled sensor tags. *Proceedings of the IEEE*. 2010; 98(9):1601-1609. http://dx.doi.org/10.1109/JPROC.2010.2049622.
15. Leung SYY and Lam DCC. Performance of printed polymer-based RFID antenna on curvilinear surface. *IEEE Transactions on Electronics Packaging Manufacturing*. 2007; 30(3):200-205. http://dx.doi.org/10.1109/TEPM.2007.901181.
16. Kido J, Kimura M and Nagai K. Multilayer white light-emitting organic electroluminescent device. *Science*. 1995; 267(5202):1332-1334. http://dx.doi.org/10.1126/science.267.5202.1332. PMid:17812607
17. Ho PK, Kim JS, Burroughes JH, Becker H, Li SF, Brown TM, et al. Molecular-scale interface engineering for polymer light-emitting diodes. *Nature*. 2000; 404(6777):481-484. http://dx.doi.org/10.1038/35006610. PMid:10761912
18. Han T-H, Lee Y, Choi M-R, Woo S-H, Bae S-H, Hong BH, et al. Extremely efficient flexible organic light-emitting diodes with modified graphene anode. *Nature Photonics*. 2012; 6(2):105-110. http://dx.doi.org/10.1038/nphoton.2011.318.
19. Berggren M, Nilsson D and Robinson ND. Organic materials for printed electronics. *Nature Materials*. 2007; 6(1):3-5. http://dx.doi.org/10.1038/nmat1817. PMid:17199114
20. Calvert P. Inkjet Printing for Materials and Devices. *Chemistry of Materials*. 2001; 13(10):3299-3305. http://dx.doi.org/10.1021/cm0101632.
21. Derby B. Inkjet printing of functional and structural materials: fluid property requirements, feature stability, and resolution. *Annual Review of Materials Research*. 2010; 40(1):395-414. http://dx.doi.org/10.1146/annurev-matsci-070909-104502.
22. Gomes TC, Constantino CJL, Lopes EM, Job AE and Alves N. Thermal inkjet printing of polyaniline on paper. *Thin Solid Films*. 2012; 520(24):7200-7204. http://dx.doi.org/10.1016/j.tsf.2012.07.119.
23. Yoon B, Ham D-Y, Yarimaga O, An H, Lee CW and Kim J-M. Inkjet printing of conjugated polymer precursors on paper substrates for colorimetric sensing and flexible electrothermochromic display. *Advanced Materials*. 2011; 23(46):5492-5497. http://dx.doi.org/10.1002/adma.201103471. PMid:22052793
24. Ballarin B, Fraleoni-Morgera A, Frascaro D, Marazzita S, Piana C and Setti L. Thermal inkjet microdeposition of pedot:pss on ito-coated glass and characterization of the obtained film. *Synthetic Metals*. 2004; 146(2):201-205. http://dx.doi.org/10.1016/j.synthmet.2004.07.006.
25. Setti L, Fraleoni-Morgera A, Ballarin B, Filippini A, Frascaro D and Piana C. An amperometric glucose biosensor prototype fabricated by thermal inkjet printing. *Biosensors & Bioelectronics*. 2005; 20(10):2019-2026. http://dx.doi.org/10.1016/j.bios.2004.09.022. PMid:15741071
26. Xu T, Jin J, Gregory C, Hickman JJ and Boland T. Inkjet printing of viable mammalian cells. *Biomaterials*. 2005; 26(1):93-99. http://dx.doi.org/10.1016/j.biomaterials.2004.04.011. PMid:15193884
27. Locklin J, Shinbo K, Onishi K, Kaneko F, Bao Z and Advincula RC. Ambipolar organic thin film transistor-like behavior of cationic and anionic phthalocyanines fabricated using layer-by-layer deposition from aqueous solution. *Chemistry of Materials*. 2003; 15(7):1404-1412. http://dx.doi.org/10.1021/cm021073f.
28. Chaidogiannos G, Petraki F, Glezos N, Kennou S and Nešpůrek S. Soluble substituted phthalocyanines for OFET applications. *Materials Science and Engineering B*. 2008; 152(1-3):105-108. http://dx.doi.org/10.1016/j.mseb.2008.06.025.
29. Šebera J, Nešpůrek S, Kratochvílová I, Záliš S, Chaidogiannos G and Glezos N. Charge carrier mobility in sulphonated and non-sulphonated ni phthalocyanines: experiment and quantum chemical calculations. *The European Physical Journal B*. 2009; 72(3):385-395. http://dx.doi.org/10.1140/epjb/e2009-00368-y.

30. Hatton RA, Blanchard NP, Stolojan V, Miller AJ and Silva SRP. Nanostructured copper phthalocyanine-sensitized multiwall carbon nanotube films. *Langmuir*. 2007; 23(11):6424-6430. http://dx.doi.org/10.1021/la070156d. PMid:17439261

31. Estrada M, Ulloa F, Avila M, Sanchez J, Cerdeira A, Castro-Carranza A, et al. Frequency and voltage dependence of the capacitance of mis structures fabricated with polymeric materials. *IEEE Transactions on Electron Devices*. 2013; 60(6):2057-2063. http://dx.doi.org/10.1109/TED.2013.2258921.

32. Lopes EM, Ywata RS, Alves N, Shimizu FM, Taylor DM, Watson CP, et al. Electrical characterization of poly(amide-imide) for application in organic field effect devices. *Organic Electronics*. 2012; 13(10):2109-2117. http://dx.doi.org/10.1016/j.orgel.2012.05.058.

33. Stallinga P, Benvenho ARV, Smits ECP, Mathijssen SGJ, Cölle M, Gomes HL, et al. Determining carrier mobility with a metal–insulator–semiconductor structure. *Organic Electronics*. 2008; 9(5):735-739. http://dx.doi.org/10.1016/j.orgel.2008.05.007.

34. Alves N and Taylor DM. Determining the interfacial density of states in metal-insulator-semiconductor devices based on Poly(3-hexylthiophene). *Applied Physics Letters*. 2008; 92(10):103312. http://dx.doi.org/10.1063/1.2897238.

35. Taylor DM and Alves N. Separating interface state response from parasitic effects in conductance measurements on organic metal-insulator-semiconductor capacitors. *Journal of Applied Physics*. 2008; 103(5):054509. http://dx.doi.org/10.1063/1.2844435.

36. Torres I and Taylor DM. Interface states in polymer metal-insulator-semiconductor devices. *Journal of Applied Physics*. 2005; 98(7):073710. http://dx.doi.org/10.1063/1.2081109.

37. Dang X-D, Plieth W, Richter S, Plötner M and Fischer W-J. Aluminum oxide film as gate dielectric for organic FETs: anodization and characterization. *Physica Status Solidi. A, Applications and Materials Science*. 2008; 205(3):626-632. http://dx.doi.org/10.1002/pssa.200723453.

38. Lu C and Chen Z. Anodic aluminum oxide-based nanostructures and devices. In: Nalwa HS, editor. *Encyclopedia of Nanoscience and Nanotechnology*. California: American Scientific Publishers; 2011. p. 235-259.

39. Hourdakis E and Nassiopoulou AG. High performance MIM capacitor using anodic alumina dielectric. *Microelectronic Engineering*. 2012; 90:12-14. http://dx.doi.org/10.1016/j.mee.2011.03.020.

40. Mahajan A, Kumar A, Singh M, Pathak D and Bedi RK. Characterization of drop casted CuTsPc films on ITO substrates. *International Journal of Nanoscience*. 2013; 12(01):1350001. http://dx.doi.org/10.1142/S0219581X13500014.

41. Sze SM. *Physics of semiconductor devices*. New York: John Wiley & Sons; 1998.